1190 *Chem. Mater.* **2005,** *17,* 1190−1198

Isovalent Doping Strategy for Manganese Introduction into III-V Diluted Magnetic Semiconductor Nanoparticles: InP:Mn

Kanchana Somaskandan,[†] Georgy M. Tsoi,[‡] Lowell E. Wenger,[§] and Stephanie L. Brock*[,†]

Department of Chemistry and Department of Physics & Astronomy, Wayne State University, Detroit, Michigan 48202, and Department of Physics, The University of Alabama at Birmingham, Birmingham, Alabama 35294-1170

Received July 23, 2004. Revised Manuscript Received December 10, 2004

III−V based diluted magnetic semiconductor (DMS) nanoparticles of $In_{(1-x)}Mn_xP$ ($x \leq 0.0135$) have been prepared by slow heating of the reagents in trioctylphosphine oxide (TOPO) or by high-temperature injection of reagents dissolved in trioctylphosphine (TOP) into hot TOPO. The materials were prepared using either Mn(II) or Mn(III) salts as dopants and the resulting nanoparticles have diameters ranging from 2.95 ± 0.39 to 4.77 ± 0.73 nm, as determined from transmission electron micrographs. Chemical analysis of surface-exchanged samples revealed the incorporation of Mn into the crystal lattice with up to 6 Mn atoms per 3.4-nm diameter particle, or the equivalence of $\sim 10^{20}$ Mn atoms/cm^3 in a zinc blende bulk lattice. The InP:Mn nanoparticles exhibited a red shift in the room-temperature photoluminescence of 0.02−0.03 eV relative to that for pure InP nanoparticles. Electron paramagnetic resonance studies suggest that the Mn atoms mostly reside near the surface and are Mn^{2+}, regardless of the oxidation state of the precursor. The magnetic susceptibility of surface-exchanged nanoparticles doped with Mn(III) exhibited a paramagnetic behavior with a magnetic moment of 5.9 μ_B/Mn atom, consistent with 5 unpaired spins ($S = 5/2$ state). The successful incorporation of isovalent Mn to produce Mn^{2+} with a corresponding hole may represent a valuable strategy for production of ferromagnetic DMS nanoparticles based on arsenide systems, where the hole is coupled to the metal center and delocalized through the pnictide framework.

Introduction

Diluted magnetic semiconductors (DMS) or semimagnetic semiconductors are solid solutions in which the semiconductor component is partially replaced by a magnetic transition metal or rare earth metal ion. In these materials, the partially filled 3d-orbitals (transition metals) or 4f orbitals (rare earths) of the metal atom supply a variety of spin-dependent properties via exchange interaction between the local moments of these ions and/or between ion moments and the charge carriers.[1] In *p*-type DMS, exchange interactions between holes in the valence band and the d-electrons of the transition metal impurity ion may lead to carrier-mediated ferromagnetism.[2−4] Although there are several classes of these compounds, including II−VI, IV−VI, II−V, and III−V semiconductors, the II−VI DMSs are the most common and extensively studied systems. Examples include ZnS:Co, ZnSe:Mn, and CdSe:Mn, which exhibit a significant range of solid solution formation with as much as 25% of the magnetic species being incorporated into the structure.[5,6] However, *p*-type doping in these II−VI based semiconductors approaching carrier concentrations of 10^{20} cm^{-3} is difficult to achieve due to charge compensation. Nevertheless, there have been recent reports of ferromagnetic behavior in thin film and bulk semiconductors of ZnO:Mn,[7,8] ZnO:V,[9] ZnO:Co,[10] and ZnTe:Cr,[11] with T_c values near or above room temperature. In many cases, the origin of ferromagnetism in these materials has been called into question, as later studies attributed the ferromagnetism to phase-segregation, or were otherwise unable to reproduce the data.[12,13]

Unlike the II−VI systems, the III−V DMS systems have limitations due to the low solubility (≤5%) of the magnetic

---

* To whom correspondence should be addressed. E-mail: sbrock@chem.wayne.edu.

[†] Department of Chemistry, Wayne State University.

[‡] Department of Physics & Astronomy, Wayne State University.

[§] Department of Physics, University of Alabama at Birmingham.

(1) Averous, M.; Balkanski, M. In *Semimagnetic Semiconductors and Diluted Magnetic Semiconductors*; Zichichi, A., Ed.; Plenum Press: New York, 1991.

(2) Ohno, H. *Science* **1998**, *281*, 951−956.

(3) Dietl, T.; Matsukara, F.; Ohno, H. *Phys. Rev. B* **2002**, *66*, 033203/1−4.

(4) Dietl, T.; Ohno, H.; Matsukura, F.; Ciber, J.; Ferrand, D. *Science* **2000**, *287*, 1019−1022.

(5) Furdyna, J. K. *J. Appl. Phys.* **1988**, *64*, R29−R64.

(6) Martin, J. L.; Goiran, M.; Golacki, Z.; Leotin, J.; Askenazy, S. *Physica B* **1995**, *211*, 388−391.

(7) Norberg, N. S.; Kittilstved, K. R.; Amonette, J. E.; Kukkadapu, R. K.; Schwartz, D. A.; Gamelin, D. R. *J. Am. Chem. Soc.* **2004**, *126*, 9387−9398.

(8) Sharma, P.; Gupta, A.; Rao, K. V.; Owens, F. J.; Sharma, R.; Ahuja, R.; Guillen, J. M. O.; Johansson, B.; Gehring, G. A. *Nat. Mater.* **2003**, *2*, 673−677.

(9) Saeki, H.; Tabata, H.; Kawai, T. *Solid State Commun.* **2001**, *120*, 439−443.

(10) Ueda, K.; Tabata, H.; Kawai, T. *Appl. Phys. Lett.* **2001**, *79* (7), 988−990.

(11) Saito, H.; Zayets, S.; Yamagata, S.; Ando, K. *J. Appl. Phys.* **2003**, *93* (10), 6796−6798.

(12) Park, J. H.; Kim, M. G.; Jang, H. M.; Ryu, S.; Kim, Y. M. *Appl. Phys. Lett.* **2004**, *84*, 1338−1340.

(13) Kundaliya, D. C.; Ogale, S. B.; Lofland, S. E.; Dhar, S.; Metting, C. J.; Shinde, S. R.; Ma, Z.; Varughese, B.; Ramanujachary, K. V.; Salamanca-Raba, L.; Venkatesan, T. *Nat. Mater.* **2004**, *3*, 709−714.

10.1021/cm048796e CCC: $30.25

species into the semiconductor matrix and the consequent segregation of a second phase during the synthesis. For example, when high concentrations of Mn were used to dope GaAs, MnAs segregation was observed.[14] However, InAs:Mn with 1.3% Mn was successfully prepared using nonequilibrium growth conditions by low-temperature molecular beam epitaxy (LT-MBE).[15] More recently, *p*-type GaAs:Mn layers have been prepared with 5.3% Mn incorporation and exhibited a T_c of 110 K.[14] In these ferromagnetic III−V based DMSs, the introduction of a hole may be considered as a consequence of isovalent doping, as Mn^{3+} is not a stable acceptor in the III−V arsenides. Instead it disproportionates to form Mn^{2+} and a hole. The proposed mechanism of ferromagnetic exchange[16] involves the creation of a half-metallic system by the introduction of these holes at the top of the valence band, which is largely As p in character. The polarization of the holes by the Mn^{2+} ion gives rise to a majority spin channel characterized by extensive mixing of the Mn 3d and As p states, and a minority spin channel, largely d-character, which occurs in the gap. The gap in the minority spin channel permits 100% spin-polarization at the Fermi level and gives rise to a ferromagnetic state. This kind of carrier-induced magnetism may be useful in potential device applications, where both the spin and charge from a single material can be effectively employed.[17] A theoretical investigation based on the Zener model has predicted ferromagnetism for a number of other zinc blende DMS materials.[4] On the basis of this analysis, InP:Mn doped with 5% Mn and 3.5×10^{20} holes per cm^3 should have a T_c of ca. 60 K. An experimental study of bulk InP implanted with Mn^+ ions at high doses produced a ferromagnetic material with a T_c of ca. 90 K.[18]

In an effort to study the influence of quantum confinement effects on DMSs and create a set of magnetic materials with the tunable optical properties characteristic of nanoparticles, many groups have investigated synthetic strategies for the incorporation of magnetic ions into semiconducting nanoparticles. These solution-phase syntheses of nanoparticulate DMS materials have been primarily focused on II−VI based compounds (CdS,[19−21] CdSe,[22−24] ZnS,[20] ZnO,[7] ZnSe[25]) because of the relative ease of preparation and facility of dopant incorporation. Although many of these materials have been found to exhibit interesting magnetooptical phenomena, none of them were ferromagnetic. Ferromagnetism has been reported in zinc oxide nanoparticles doped with transition metals, such as Ni^{2+} and Co^{2+}, but ferromagnetic exchange was only observed in aggregated samples, and not in discrete nanoparticles or well crystallized bulk samples.[26−29] Thus, it is not clear whether the ferromagnetic exchange arises from interactions of diluted spins or is related to interactions from segregated ions at grain boundaries. In contrast, very little work has been performed on III−V DMSs prepared from solution methods; the focus has been primarily on thin films or nanoparticles prepared by MBE. Many III−V based thin film heterostructures have been reported to date.[17,30−32] The first report of III−V-based DMS quantum dots described InAs:Mn nanostructures grown on a GaAs substrate using MBE.[33] However, these quantum dots adopted a range of morphologies with a broad size distribution. A second study on the same system confirmed that the particles were nanoparticulate in nature but relatively large in size (∼60 nm) with a purported T_c of 400 K.[34] Very recently, the solution-phase synthesis of InAs:Mn nanoparticles (4−10 nm) with a fairly narrow size distribution has been reported using Mn(II) precursors.[35] These samples were paramagnetic and showed reduced moments more consistent with four unpaired spins. These characteristics were attributed to the Mn dopant acting as an acceptor in an overall *n*-doped system.

The question of how quantum confinement effects will influence the magnetic properties in DMSs has been treated computationally for the case GaAs:Mn. Despite a significant perturbation in the energy of the bands and a decrease in bandwidth as the confinement is enhanced, the half-metallic state is retained for particles down to 2.5 nm in diameter.[16] However, these properties are predicated on having a *p*-type doped system. Therefore, an essential factor in the creation of ferromagnetic DMS nanoparticles based on III−V architectures is the ability to hole dope.

The preparation of III−V DMS nanoparticles by solution-phase precipitation techniques permits control of the con-

---

(14) Matsukara, F.; Ohno, H.; Shen, A.; Sugawara, Y. *Phys. Rev. B* **1998**, *57*, R2037−R2040.
(15) Munekata, H.; Ohno, H.; von Molnar, S.; Segmuller, A.; Chang, L. L.; Esaki, L. *Phys. Rev. Lett.* **1989**, *63*, 1849−1852.
(16) Sapra, S.; Sarma, D. D.; Sanvito, S.; Hill, N. A. *Nano Lett.* **2002**, *2*, 605−608.
(17) Reed, M. L.; el-Masry, A.; Stadelmaier, H. H.; Ritums, M. K.; Reed, M. J.; Parker, C. A.; Roberts, J. C.; Bedair, S. M. *Appl. Phys. Lett.* **2001**, *79*, 3473−3475.
(18) Shon, Y.; Lee, W. C.; Park, Y. S.; Kwon, Y. H.; Lee, S. J.; Chung, K. J.; Kim, H. S.; Kim, D. Y.; Fu, D. J.; Kang, T. W.; Fan, X. J.; Park, Y. J.; Oh, H. T. *Appl. Phys. Lett.* **2004**, *84*, 2310−2312.
(19) Bandaranayake, R. J.; Lin, J. Y.; Jiang, H. X.; Sorensen, C. M. *J. Magn. Magn. Mater.* **1997**, *169*, 289−302.
(20) Malik, M. A.; O'Brien, P.; Revaprasadu, N. J. *J. Mater. Chem.* **2001**, *11*, 2382−2386.
(21) Counio, G.; Gacoin, T.; Boilot, J. P. *J. Phys. Chem. B* **1998**, *102*, 5257−5260.
(22) Mikulec, F.; Kuno, M.; Bennati, M.; Hall, D. A.; Griffin, R. G.; Bawendi, M. G. *J. Am. Chem. Soc.* **2000**, *122*, 2532−2540.
(23) Hanif, K. M.; Meulenberg, R. W.; Strouse, G. F. *J. Am. Chem. Soc.* **2002**, *124*, 11495−11502.
(24) Raola, O. E.; Strouse, G. F. *Nano Lett.* **2002**, *2*, 1443−1447.
(25) Norris, D. J.; Yao, N.; Charnock, F. T.; Kennedy, T. A. *Nano Lett.* **2001**, *1*, 3−7.
(26) Radovanovic, P. V.; Gamelin, D. R. *Phys. Rev. Lett.* **2003**, *91*, 157202/1−4.
(27) Schwartz, D. A.; Norberg, N. S.; Nguyen, Q. P.; Parker, J. M.; Gamelin, D. R. *J. Am. Chem. Soc.* **2003**, *125*, 13205−13218.
(28) Lawes, G.; Risbud, A. S.; Ramirez, A. P.; Seshadri, R. *Los Alamos National Laboratory Preprint Archive, Condensed Matter* **2004**, arXiv: cond-mat/0403196, 1−5.
(29) Risbud, A. S.; Spaldin, N. A.; Chen, Z. Q.; Stemmer, S.; Seshadri, R. *Phys. Rev. B* **2003**, *68*, 205202/1−7.
(30) Soo, Y. L.; Huang, S. W.; Ming, Z. H.; Kao, Y. H.; Munekata, H.; Chang, L. L. *Phys. Rev. B* **1996**, *53*, 4905−4909.
(31) Kawakami, R. K.; Johnston-Halpperin, E.; Chen, L. F.; Hanson, M.; Guébels, N.; Speck, J. S.; Gossard, A. C.; Awschalom, D. D. *Appl. Phys. Lett.* **2000**, *77*, 2379−2381.
(32) Overberg, M. E.; Gilla, B. P.; Thaler, G. T.; Abernathy, C. R.; Pearton, S. J.; Theodoropoulou, N. A.; McCarthy, K. T.; Arnason, S. B.; Hebard, A. F.; Chu, S. N. G.; Wilson, R. G.; Zavada, J. M.; Park, Y. D. *J. Vac. Sci. Technol., B* **2002**, *20*, 969−973.
(33) Guo, S. P.; Ohno, H.; Shen, A.; Matsukara, F.; Ohno, Y. *Appl. Surf. Sci.* **1998**, *132*, 797−802.
(34) Jeon, H. C.; Jeong, Y. S.; Kang, T. W.; Kim, T. W.; Chung, K. J.; Chung, K. J.; Jhe, W.; Song, S. A. *Adv. Mater.* **2002**, *14*, 1725−1728.
(35) Stowell, C. A.; Wiacek, R. J.; Saunders, A. E.; Korgel, B. A. *Nano Lett.* **2003**, *3*, 1441−1447.

centration and oxidation state of precursors, thereby potentially controlling the extent and kind of doping in these materials. We surmised that *p*-type doping combined with Mn^{2+} doping could be achieved by isovalent substitution of III−V semiconductors through the use of Mn(III) salts or complexes. Herein we test this premise for InP:Mn, compare the influence of precursor oxidation state on resulting properties, and consider the validity of this general approach for the synthesis of III−V ferromagnetic semiconductors.

Experimental Section

Synthesis. All starting materials were stored in an argon-filled glovebox and reactions were conducted using rigorous airfree procedures, either in a glovebox or on a Schlenk line. Trioctylphosphine oxide (TOPO, Aldrich, 90%), toluene, methanol, and hexane (Fisher) were distilled before use. Trioctylphosphine (TOP, Aldrich, 90%), indium(III) chloride ($InCl_3$, Alfa Aesar, 99.99%), tris(trimethylsilyl)phosphine ($P(SiMe_3)_3$, nitrogen flushed, Acros, 98%), manganese(II) chloride ($MnCl_2$, Aldrich, 99.99+%), manganese(II) iodide (MnI_2, Acros, 99%), manganese(III) acetylacetonate ($Mn(acac)_3$, Aldrich, tech.), and manganese(III) 2,2,6,6,-tetramethyl-3,5-heptanedionate ($Mn(TMHD)_3$, Strem, 99%) were used without further purification.

$In_{(1-x)}Mn_xP$ particles were synthesized using (1) a high-temperature dehalodesilylation route (slow heating) and (2) a high-temperature injection method.

(1) High-Temperature Dehalodesilylation Route. $InCl_3$ (0.90 mmol) and 0.10 mmol Mn salt or complex ($x = 0.10$) were combined with 10 mL of TOP in an argon-purged Schlenk flask. This mixture was slowly heated to 260−270 °C and was allowed to stabilize at this temperature for 30−60 min. $P(SiMe_3)_3$ (1.0 mmol) was subsequently injected into the reaction mixture via syringe and the solution was heated for another 1−2 h.

(2) High-Temperature Injection Route. $InCl_3$ (0.90 mmol) was combined with 12.5 mL of TOPO in an argon-purged Schlenk flask and heated to 200 °C for about 30 min. The temperature was subsequently increased to 300 °C, and maintained for ~1 h. Solutions of 1.0 mmol $P(SiMe_3)_3$ in 3 mL of TOP and 0.10 mmol Mn salt in 5 mL of TOP were prepared in the drybox, combined, and subsequently cannulated into the hot TOPO−$InCl_3$ mixture. The reaction temperature was adjusted to 260 °C and the reaction was maintained at this temperature for 2−3 h. As $MnCl_2$ dissolves very slowly in TOP at room temperature, the $MnCl_2$/TOP solution was gently heated to 80−100 °C until all of the solid had dissolved, then allowed to return to room temperature before combining with the $P(SiMe_3)_3$ solution and injecting into the hot TOPO.

The TOP and/or TOPO solutions were subsequently slowly cooled to 60 °C and diluted with an equal volume of chloroform (for method 1) or toluene (for method 2). Fractions were separated by adding increased amounts (from 1−4 mL) of ethanol (method 1) or methanol (method 2) into the mixture, followed by centrifugation. Generally, about 4−6 precipitated fractions were isolated in all cases. Portions of the separated particles were redissolved in toluene, reprecipitated, and analyzed as described below. These data were compared to another portion from the same fraction subjected to pyridine exchange. TEM, XRD, and magnetic susceptibility were acquired only on the second precipitated fraction from each synthesis, whereas optical data were acquired on a range of fractions from each method. Both methods 1 and 2 were conducted similarly for $x = 0.25$ using 0.75 mmol $InCl_3$ and 0.25 mmol Mn salt.

In some cases, nanoparticles were coated with a second shell of InP to make isocrystalline core−shell materials.[36] After surface exchange with pyridine (vide infra), nanoparticles were redispersed in TOPO and separate solutions of 0.10 mmol $InCl_3$ in TOP and 0.10 mmol $P(SiMe_3)_3$ in TOP were added dropwise. The resultant solution was allowed to stir at 260 °C for 30 min and the isocrystalline particles were isolated as before.

Surface Ligand Exchange. Surface ligand exchange with pyridine was achieved by dissolving 0.3−0.5 g of TOP/TOPO capped particles in 7−10 mL of pyridine and heating to 60 °C for 15 min.[37] Excess hexane was added until cloudiness was observed and the suspension was subsequently centrifuged. This process was repeated at least 3 times and the resultant precipitate was kept inside the drybox until used for further characterization and analyses. Alternatively, the precipitate obtained from size-selective separation was dissolved in approximately 15 mL of pyridine, allowed to stir for about 24 h at room temperature,[35] and precipitated once with excess hexane. The multiple step surface exchange was performed on particles prepared by method 2 whereas the single step method was employed on particles prepared from method 1.

X-ray Powder Diffraction. X-ray diffraction patterns on InP:Mn surface-exchanged particles isolated from the second precipitated fraction were collected with a Rigaku Ru200B 12 kW diffractometer using Cu Kα radiation (1.54056 Å) at 40 kV and 150 mA. A slurry of nanoparticles in methanol was deposited on a quartz (0001) low background holder and allowed to air-dry prior to the acquisition of diffraction patterns. The crystallite sizes were calculated from an average of values obtained by using the Scherrer equation on the three prominent reflections. The errors represent the standard deviation in these measurements.[38]

Transmission Electron Microscopy (TEM). TEM images on surface-exchanged particles of InP:Mn were taken with a JEOL 2010 transmission electron microscope at the University of Michigan Electron Microbeam Analysis Laboratory (EMAL) operating at 200 kV. Samples were dissolved in pyridine and a drop was placed onto a 200 mesh TEM copper grid coated with a thin amorphous carbon film. The grid was prepared in a glovebox and left under ambient conditions for 2−3 h to evaporate the solvent. Grids were transported to the microscope in a vacuum-sealed desiccator.

UV/Visible Spectroscopy. UV/Visible spectra were obtained on InP and InP:Mn samples of nominally 3.2-nm diameter particles (as determined from TEM) using a Hewlett-Packard 8452A diode array spectrophotometer. Samples were dissolved in either pyridine or toluene and the absorption was measured using 10-mm quartz cuvettes with pure solvent as the background.

Luminescence Spectroscopy. Photoluminescence measurements were taken on samples of InP and InP:Mn particles of nominally 3.2-nm diameter (as determined from TEM) with a SPEX Fluoromax 2 spectrofluorometer using a 12 μA photodiode as a reference detector and DM 3000F software. Isolated particles from different fractions were dissolved in toluene and the solutions were diluted prior to the measurements. All the measurements were done at room temperature with an excitation wavelength of 530 nm.

Electron Paramagnetic Resonance (EPR) Spectroscopy. EPR was performed on as-prepared and surface-exchanged particles of InP and InP:Mn isolated from the second precipitated fraction using a Bruker EMX spectrometer operating at 9.44 GHz (X-band) microwave frequency. The spectra were collected using 10.010 mW power. Dry, solid samples were placed in quartz tubes and

---

(36) Radovanic, P. V.; Gamelin, D. R. *J. Am. Chem. Soc.* **2001**, *123*, 12207−12214.

(37) Murray, C. B.; Norris, D. J.; Bawendi, M. G. *J. Am. Chem. Soc.* **1993**, *115*, 8706−8715.

(38) Cullity, B. D. *Elements of X-ray Diffraction*; Addison-Wesley Publishing Company: Reading, MA, 1978.

Table 1. Various InP:Mn Nanoparticle Samples with Preparative Method, Dopant, Fraction Isolated from Size Selective Precipitation (SSP) Employed, Method of Surface Exchange, and Quantity of Mn Detected by ICP-MS (±10% of the value)

sample	synthetic method	dopant	fraction from SSP	method of surface exchange	molar % of Mn
DMS10II-A	slow heating	$MnCl_2$	second	stirred 24 h in pyridine	0.07
DMS10II-B	slow heating	MnI_2	second	stirred 24 h in pyridine	0.08
DMS10III-A	slow heating	$Mn(acac)_3$	second	stirred 24 h in pyridine	0.12
DMS10III-B	slow heating	$Mn(TMHD)_3$	second	stirred 24 h in pyridine	0.37
DMS25II-A	slow heating	$MnCl_2$	second	stirred 24 h in pyridine	0.02
DMS25III-A	slow heating	$Mn(acac)_3$	second	stirred 24 h in pyridine	1.35

measurements were taken at temperatures ranging from 115 to 185 K using a liquid nitrogen cryostat. The data were not normalized with respect to Mn concentration.

Chemical Analysis. Quantitative analyses of In, P, and Mn content were performed on surface-exchanged particles of InP:Mn isolated from the second precipitated fraction. Samples were prepared by dissolution in a 10% aqua regia solution and analyzed by RTI Laboratories, Inc. (Livonia, MI) using inductively coupled plasma−mass spectrometry (ICP−MS).

Magnetic Susceptibility. DC magnetic susceptibility studies were performed using a Quantum Design model MPMS-5S SQUID magnetometer. Magnetic susceptibility-vs.-temperature data were acquired from 5 to 300 K in an applied field of 0.5 T and magnetization-vs.-applied field measurements were taken at 5 and 300 K. Samples were sealed in ca. 15-cm long quartz tubes under vacuum prior to the magnetic measurements in order to prevent any air oxidation of the material.

Results

Synthesis. Two methods were adopted for the synthesis of InP:Mn nanoparticles: slow heating of reagents and high-temperature injection. Using the slow heating method, $InCl_3$, the Mn source, and TOP were heated together up to 260 °C and $P(SiMe_3)_3$ was injected into the reaction mixture. Alternatively, in the injection method, $InCl_3$ was initially heated with TOPO up to 300 °C, and a TOP solution of Mn precursor and phosphine was injected into the reaction mixture. The resultant solutions in both cases were brown when a high concentration of Mn salts (25%) was used, and maroon when low concentrations were used (10%). The 10% solutions were visually similar to solutions of undoped InP nanoparticles. The particles were isolated using size-selective precipitation, and fractions exhibited a gradation of color from darker to lighter, consistent with larger particles making up earlier fractions. The isolated precipitates were waxy in texture, attributed to the coprecipitation of TOP/TOPO. Surface ligand exchange reactions with pyridine resulted in fine, free-flowing dark powders after isolation. In some cases, these were redispersed in TOPO and "capped" with an additional layer of InP to ensure that any residual surface manganese was adopted into the core of the particle.[36] Attempts to prepare particles using Mn concentrations of greater than 30% of the In concentration resulted in intractable solutions from which it was not possible to induce precipitation.

The prepared materials will be denoted as DMS25 and DMS10 for samples prepared with 25% and 10% Mn salts, respectively; and the Roman numerals II and III will be used to indicate the oxidation state of the manganese precursor: II for divalent Mn in $MnCl_2$ or MnI_2, and III for trivalent Mn in $Mn(acac)_3$ or $Mn(TMHD)_3$. The oxidation state of manganese detected in the InP nanoparticles will be designated as 2+ or 3+. The influence of the synthesis method, slow heating (method 1) or high-temperature injection (method 2), did not have any substantive effects on the properties of the final product, nor did the addition of an isocrystalline shell of InP to preformed InP:Mn particles. Thus the results presented in this paper are from samples prepared by the slow heating route (method 1, see Table 1) and primarily use $MnCl_2$ as the divalent Mn precursor and $Mn(acac)_3$ as the trivalent precursor. No significant difference in the uptake level or physical properties was observed when MnI_2 was employed in lieu of $MnCl_2$. However, $Mn(TMHD)_3$ did not result in consistent uptake values, although the physical properties were essentially identical to those observed when $Mn(acac)_3$ was employed.

Structural Characterization. Surface-exchanged and -unexchanged doped nanoparticles prepared under different synthesis conditions and with different dopants were initially characterized using X-ray powder diffraction (XRD). In all cases the patterns were characteristic of cubic InP with reflections positioned at $2\theta = 26°$, 44°, and 51° for the (111), (220), and (311) crystal planes, respectively, (Figure 1a) with no apparent shift in peak position for doped samples as compared to the parent InP phase. Electron micrographs acquired from TEM studies indicated that the particles have a uniform spherical morphology (Figure 1b).

Particle Size Analysis. The peaks in the XRD patterns show broadening characteristic of nanosized crystalline domains. Crystallite sizes were estimated from the diffraction peak broadening (full-width at half-maximum) by application of the Scherrer equation and are given in Table 2 for typical samples. The average particle size was also determined from statistical analysis on large fields of nanoparticles in low magnification images from TEM (Table 2). The standard deviations based on 300−400 particles counted ranged from 8 to 16%. This is indicative of narrow-size distributions and typical for pure InP synthesized by this procedure.[39] The size estimated from peak broadening of the X-ray diffraction patterns for most samples was smaller than that obtained from TEM, although generally within the standard deviation. The exception was DMS25III-A, in which the XRD data significantly underestimated the size as compared to that deduced from TEM (Table 2), which suggests poorer crystallinity in this material.

Elemental Analysis. Quantitative analyses were performed on pyridine-exchanged samples and the data are presented in Table 1. These samples showed anywhere from a 15−95% loss of Mn relative to unexchanged samples, consistent

---

(39) Guzelian, A. A.; Katari, J. E. B.; Kadavanich, A. V.; Banin, U.; Hamad, K.; Juban, E.; Alivisatos, A. P.; Wolters, R. H.; Arnold, C. C.; Heath, J. R. *J. Phys. Chem. B* **1996**, *100*, 7212−7219.

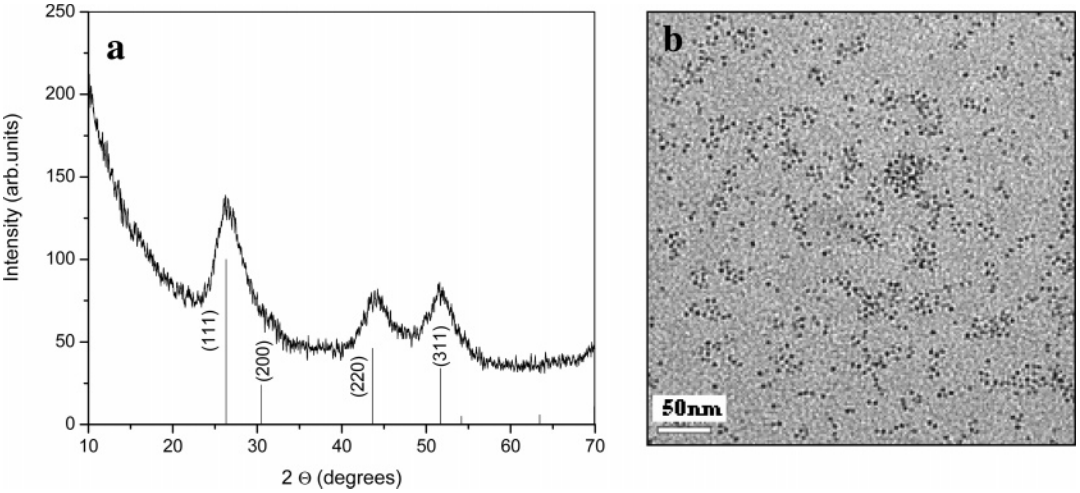

Figure 1. (a) XRD pattern of DMS10III-A nanoparticles and line diagram showing the positions and relative intensities for reflections of InP. (b) Corresponding TEM image of DMS10III-A with an average particle size of 3.39 ± 0.28 (± 8%).

Table 2. Particle Sizes for Surface-Exchanged Samples from Table 1 and the Average Number of Mn Atoms Per Particle[a]

	Particle Diameter (nm)		average number of Mn atoms per nanoparticle
sample	XRD	TEM	
DMS10II-A	3.46 ± 0.73	3.93 ± 0.56	0.4
DMS10III-A	3.00 ± 0.20	3.39 ± 0.28	0.5
DMS25II-A	4.50 ± 0.60	4.77 ± 0.73	0.3
DMS25III-A	2.60 ± 0.36	3.42 ± 0.56	5.6
InP	3.80 ± 0.88	3.73 ± 0.40	NA

[a] Diameters were calculated from XRD patterns using the Scherrer equation or measured from images acquired by transmission electron microscopy. Mn atoms per particle were computed based on the TEM data along with the ICP-MS data from Table 1.

with removal of surface-bound impurity ions during the exchange process. Under identical conditions it was possible to incorporate larger quantities of Mn(III) ions than Mn(II) ions, although this may also be a function of the difference in counterions (i.e., acac vs Cl) employed in these syntheses. When higher concentrations of Mn(III) were used in the synthesis, the degree of incorporation was significantly better. The highest degree of incorporation obtained corresponds to an average of ∼6 Mn atoms per 3.4-nm diameter particle, which would correspond to a bulk dopant level of $\sim 10^{20}$ Mn/cm^3.

Optical Absorption and Photoluminescence. Absorption and photoluminescence (PL) spectra were obtained on InP:Mn and InP nanoparticles of approximately 3.2-nm diameter, as estimated from TEM measurements (Figure 2a). All samples had absorption onsets significantly blue-shifted from the bulk band gap value (1.35 eV), consistent with quantum confinement effects. The band-edges (estimated from the absorption onset) were 1.73, 1.77, and 1.76 eV for DMS25III, DMS25II, and InP samples, respectively. The peak corresponding to the first excitonic excitation was poorly resolved in the pure InP sample relative to the InP:Mn samples, making the positions of the absorption maxima more difficult to estimate. The PL spectra acquired at an excitation wavelength of 530 nm revealed a sharp feature near the absorption maxima for each of the samples, with the PL peaks for DMS25III and DMS25II samples being slightly red-shifted from the parent InP phase (1.92 and 1.93 vs 1.95 eV), which corresponds to a reduction in energy of about 0.02−0.03 eV. As observed for pure InP nanoparticles, the DMS nanoparticles demonstrated a clear red shift in the photoluminescence with increasing particle size (Figure 2b).

Magnetic Properties. The speciation of Mn ions in InP:Mn nanoparticles was evaluated using EPR and dc magnetic susceptibility experiments. Prior to the surface washing, a simple isotropic signal is observed in the EPR (Figure 3a), which is attributed to coupling between a large number of Mn centers. After surface exchange, characteristic six-line hyperfine splitting patterns centered at $g \approx 2.0$ indicative of Mn^{2+} were observed in all cases, even when the precursor starting material was Mn(III) (Figure 3b). This hyperfine splitting pattern is typically superimposed over an isotropic pattern with the spectra for the DMS10II-A samples displaying relatively sharper peaks (greater depth) than those for the DMS10III-A samples, which in turn were sharper than those for DMS25III-A. Thus, the isotropic component contribution relative to the hyperfine splitting contribution scales with the degree of Mn incorporation. The hyperfine splitting constant values (Table 3) do not change significantly as a function of degree of incorporation, or upon the addition of an isostructural shell of InP to the previously doped nanoparticles (Supporting Information). Samples prepared with Mn(II) precursors had slightly smaller splitting constants than those obtained from Mn(III) precursors. The DMS 10III-A sample had two discernible *A* constants, a characteristic found in a number of other samples.

The temperature-dependent magnetic susceptibility measurements for all samples revealed an increasing susceptibility with decreasing temperature, suggestive of a paramagnetic behavior (Figure 4), and susceptibility magnitudes greater than that measured for pure InP nanoparticles, indicating a magnetic response due to the presence of the Mn ions. Initial attempts to fit the raw data to a Curie−Weiss equation were unsuccessful due to contributions from the sample holder and the InP matrix dominating at higher temperatures. Consequently, a fit including a temperature-independent contribution was attempted (eq 1)

$$\chi = \chi_P + \alpha = C/(T + \theta) + \alpha \qquad (1)$$

where α represents the temperature-independent component,

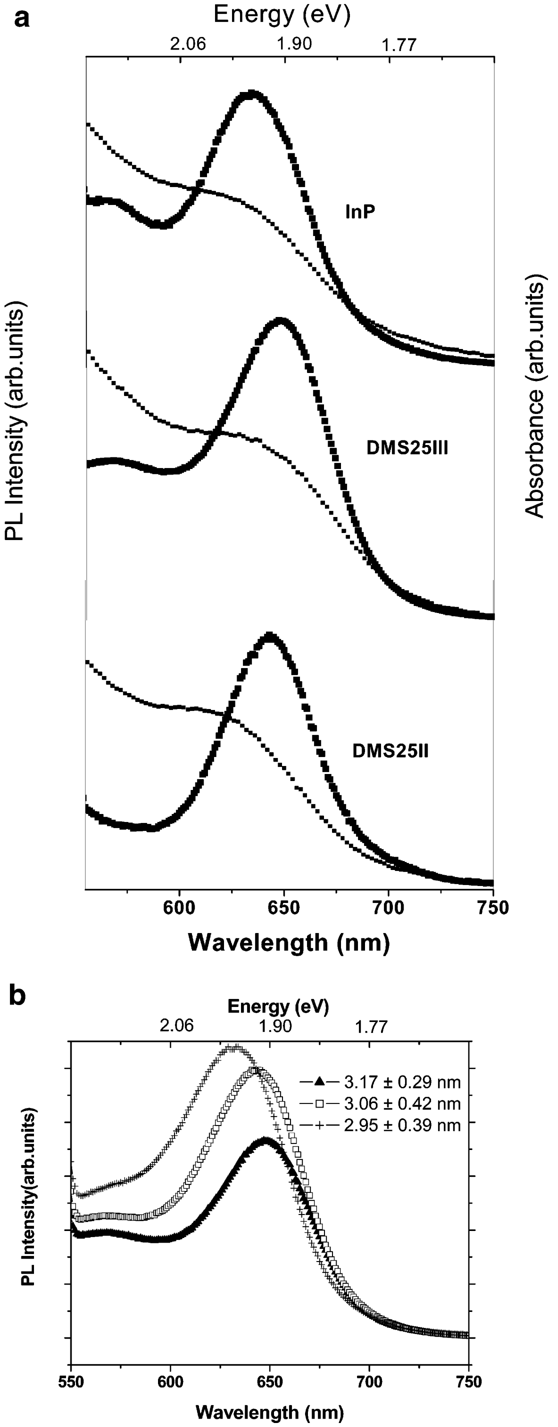

Figure 2. (a) Absorption and photoluminescence spectra of ~3.2-nm diameter InP, DMS25III, and DMS25II nanoparticles. (b) Photoluminescence spectra of selected fractions of surface-exchanged DMS25III samples. DMSII and DMSIII samples were prepared using $MnCl_2$ or $Mn(acac)_3$, respectively, via the slow heating route (method 1). The feature near 575 nm in the photoluminescence is due to the solvent (toluene).

C is the paramagnetic Curie constant, and θ is the Curie−Weiss temperature. Plots of χ vs. T^{-1} yielded fairly straight lines with intercepts α (see Supporting Information) for fits over the entire temperature range for the DMS25III-A sample and only over the temperature range below 50 K for all other InP:Mn samples. This is due to the sample holder and InP susceptibilities dominating the measured susceptibility above 50 K in these lower Mn-doped samples and being no longer truly "temperature independent". After subtracting the α term from the DMS25III-A data, a subsequent plot of χ_P^{-1} vs. T exhibited a linear behavior (Figure 4 inset) from which the effective moment of 5.9 Bohr magnetons (BM) per Mn ion was determined from the slope and a Curie−Weiss temperature θ of −0.17 K was determined from the intercept. This moment is very close to the spin-only value of $S = 5/2$ and is consistent with Mn^{2+} in a high spin (d^5) configuration.

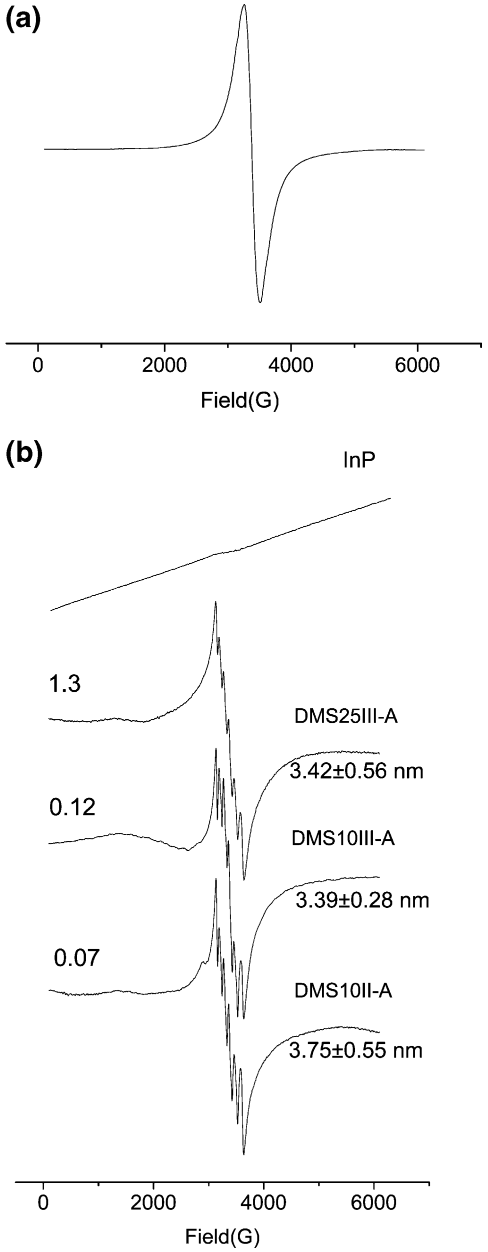

Figure 3. EPR spectra of (a) an unexchanged sample of DMS25III-A showing the characteristic isotropic signal and (b) InP and surface-exchanged DMS25III-A, DMS10III-A, and DMS10II-A samples taken at temperatures ranging from 115 to 185 K. Manganese molar concentrations of exchanged samples as determined from ICP-MS are indicated to the left of the spectra. The sloping baseline for InP is found to be consistent from sample to sample, and may be due to the presence of adventitious dopant ions with integer spins giving rise to poorly defined EPR signals with broad line widths.

Table 3. Calculated *g* and Hyperfine Splitting Constant (*A*) Values Determined by EPR for Selected Surface-Exchanged Samples from Table 1

sample	*g* value	$A \times 10^{-4}$ cm^{-1}
DMS10II-A	2.025	82.5
DMS10III-A	2.022	84.7, 87.6
DMS25III-A	2.026	84.5

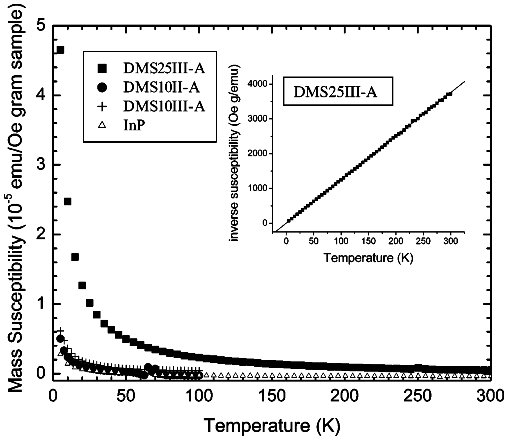

Figure 4. Temperature-dependent magnetic susceptibility per gram of the surface-exchanged DMS25III-A, DMS10III-A, DMS10II-A, and pure InP nanoparticle samples. The inset shows the inverse susceptibility plot after subtraction of the temperature-independent component (filled squares are data, the line represents the linear fit) for the DMS25III-A sample.

Although the θ value from the least-squares fit was small and negative ($\theta = -0.17 \pm 0.2$ K), the large uncertainty precludes drawing the conclusion that weak antiferromagnetic exchange actually exists between the unpaired spins. Moreover, since the θ value for the largest Mn-doped sample (DMS25III-A) is negligible compared to the temperature range of these measurements, it is reasonable to assume that the θ values are also negligible ($\theta \approx 0$) for the other lower Mn-doped samples as well. Thus the slopes of the χ vs. T^{-1} plots would be directly proportional to the paramagnetic Curie constant and the effective moment of the Mn ions. The resulting effective moments per Mn ion from these slopes were found to range from 7.6 to 5.1 μ_B for DMS10II-A and 7.4 to 5.4 μ_B for DMS10III-A with the lower value resulting from subtracting the "paramagnetic moment" slope measured for the pure InP sample. While these effective moment values also seem to be consistent with Mn in these very lowest-dopant samples being in a high spin (d^5) configuration, the large uncertainty arising from the actual Mn content detected by ICP-MS, from the very weak magnetic response measured, and from the relatively large "paramagnetic" correction due to non-Mn impurities and the sample holder, precludes a more definitive assertion as to the spin state in these two samples.

Discussion

The main problem with DMS syntheses of III−V based materials has been the tendency for phase segregation of MnPn (Pn = P, As) due to the low solubility of Mn in the III−V matrix. The use of low-temperature MBE methods (<350 °C) along with relatively low concentrations of Mn (<5%) has permitted the formation of metastable solid solutions in thin film form.[2] Similarly, the syntheses in this study take advantage of rapid arrested precipitation reactions in coordinating solvents to form nanoparticles at similarly low-temperatures. However, a recurrent problem with nanoparticle synthesis is the segregation of impurities to the surface, which is facile, due to the short diffusion length-scales in the particles. In many II−VI DMS nanoparticulate syntheses reported to date, only a small fraction of the magnetic ions introduced are actually incorporated into the semiconductor lattice, while the rest either stay on the particle surface or segregate into another phase.[20] To ensure maximum uptake, we employed large excesses of the dopant ion in the synthesis, up to 25% of the amount of In. Unfortunately, higher concentrations resulted in solutions from which no nanoparticles could be precipitated, a behavior similar to what we have observed when trying to make manganese phosphides using the same divalent and trivalent manganese precursors with $P(SiMe_3)_3$.[40]

The surface of the synthesized particles was subsequently exchanged with pyridine to replace the TOP and TOPO capping groups and wash away surface manganese species. (TOPO, in particular, is known to be an excellent complexing agent for transition metal ions,[41] thereby acting to trap Mn^{2+} at the surface of the particle). Up to 95% of the Mn in the sample is lost during this ligand exchange step, leaving up to 1.35% Mn incorporated (for an Mn(III) precursor) into the nanoparticle's interior. This corresponds to an average of 6 Mn ions per 3.4-nm diameter particle, or an equivalent bulk concentration of about 10^{20} Mn atoms/cm^3, which is at least an order of magnitude greater than the maximum Mn concentration reported in bulk InP (3×10^{17} to 7×10^{18} cm^{-3}).[42] The formation of a separate phase such as MnP can be ruled out, as we have established that reactions between $P(SiMe_3)_3$ and $Mn(acac)_3$ or $MnCl_2$ do not produce metal phosphides.[40,43]

The data from X-ray powder diffraction (XRD) confirm the formation of a zinc blende structure in these InP:Mn nanoparticles. There is no evident shift in lattice parameters, consistent with the low degree of doping observed, although very small shifts in peak positions may be obscured by the breadth of the peaks as a result of the small size of the crystalline domains. The particle sizes calculated from XRD compare favorably with those obtained from TEM imaging (2.5−5 nm), except in cases where the largest amounts of Mn were incorporated. When ca. 1% Mn or more was incorporated, XRD analysis tended to underestimate the size, which suggests a possible decrease in the overall crystallinity of the sample, perhaps due to the disruption of the lattice at high concentrations of Mn. Likewise, it is also possible that some small degree of shift in the lattice parameters, or a range of lattice parameters due to nonuniform composition throughout the sample, gives rise to the breadth in the peaks.

Room-temperature photoluminescence studies reveal only subtle differences between the doped samples and pure InP for samples of similar size and polydispersity. The apparent red-shift in both the Mn(II) and Mn(III) samples may be indicative of the presence of an acceptor level in the gap; however, the magnitude of the shift is very small (<0.03 eV) compared to the value of ~0.2 eV reported for a doped InP:Mn crystal.[2] This may be due to a shift in the position of the d-band due to hybridization and geometrical effects

---

(40) Perera, S. C.; Tsoi, G.; Wenger, L. E.; Brock, S. L. *J. Am. Chem. Soc.* **2003**, *125*, 13960−13961.

(41) Burgard, M.; Prevost, M. *Phosphorus Sulfur* **1983**, *18*, 319−322.

(42) Masterov, V. F.; Małtsev, Y. V.; Sobolevskii, V. K. *Sov. Phys. Semicond.* **1981**, *15*, 1235−1237.

(43) Brock, S. L.; Perera, S. C.; Stamm, K. L. *Chem. Eur. J* **2004**, *10*, 3364−3371.

in the nanocrystal, or to the presence of additional impurities. An additional possibility is that the chromophore size parallels more closely the size of the crystalline component, rather than the overall particle size estimated from TEM images. As the crystallinity is apparently reduced at high dopant concentrations, the doped crystals may in fact be smaller in size than their undoped counterparts, and the true-red-shift greater than the apparent shift of 0.03 eV. As can be seen in Figure 2b, the photoluminescence maxima are very sensitive to even small shifts in size for InP:Mn nanoparticles.

It is interesting to note that regardless of whether Mn(II) or Mn(III) is employed as a dopant ion, the EPR data demonstrate a six-line hyperfine splitting pattern characteristic of a diluted d^5 Mn^{2+} center. The incorporation of a simple substitutional Mn^{3+} as a d^4 ion would be expected to result in an $S = 2$ state and would be EPR silent. This suggests that the isovalent Mn(III) precursor forms Mn^{2+} during its incorporation and, concomitantly, a hole; i.e., ion doping and hole doping are simultaneously occurring in the sample. Disproportionation of Mn^{3+} to yield Mn^{2+} and a hole is a well-established process in III−V DMSs.[42,44,45] When the hole is localized in the valence band (producing an anionic acceptor, d^5) weak antiferromagnetic interactions result; however, when the hole is coupled to Mn^{2+} and delocalized (producing a neutral acceptor, $d^5 + h$), a half-metal state can be formed that gives rise to carrier induced ferromagnetism.[46] Both acceptors should produce characteristic resonances in the EPR, with the d^5 anionic acceptor (A^-) giving rise to a signal at $g = 2.0$ and the neutral $d^5 +$ h acceptor (A^0) giving signals at $g = 2.77$ and 5.72.[44] Resonances were observed at $g = 2.0$, 2.8, and 6.5 in heavily doped GaAs:Mn crystals, and were attributed to the presence of both the A^- and A^0 acceptors.[44] In contrast, only A^- (d^5) centers were observed in GaAs:Mn epilayers and the absence of the A^0 lines has been attributed to a reduction in the hole binding energy due to the presence of a high concentration of holes in these samples, which can effectively screen the A^- center.[44] Photostimulated EPR studies of bulk GaP:Mn indicated a combination of d^4 and A^- (d^5) centers,[46] whereas InP:Mn EPR data were consistent with an A^- center with $g = 2.01$ and $A = 55 \times 10^{-4}$ cm^{-1}.[42,45] Frequently, the sextet at $g = 2.0$ is poorly resolved and lacking in depth, and this is attributed to interactions between Mn centers giving rise to a large isotropic component to the signal.[47]

Our EPR results indicate that only ionized d^5 centers are present in our samples. Furthermore, the hyperfine splitting constant (A) values are larger than 80×10^{-4} cm^{-1}, regardless of the dopant precursor, Mn(II) or Mn(III), or the dopant concentration. Mn^{2+} ions in a covalently bound tetrahedral site in the cubic lattice would typically be expected to exhibit A values in the range of 50×10^{-4} to 65×10^{-4} cm^{-1},[42,48,49] whereas values of 90×10^{-4} cm^{-1} have been attributed to ionic Mn^{2+} (surface bound Mn, in the case of nanoparticles) or to Mn^{2+} located on an interstitial site.[50] For InAs:Mn nanoparticles, a value of 74×10^{-4} cm^{-1} was obtained and attributed to Mn being in an ionic tetrahedral environment.[35]

Since the surfaces of our InP:Mn particles were exchanged well with pyridine, surface-bound Mn^{2+} should not be present in large amounts. To confirm this, we used a modification of the isocrystalline core−shell method of Gamelin and coworkers.[36] We find that the nominal value of $A = 83{-}85 \times 10^{-4}$ cm^{-1} does not change upon the addition of a pristine "shell" of InP around the previously doped particles, which would be expected to convert surface Mn^{2+} to internal Mn^{2+}. Similarly, Mn ions incorporated into CdSe are reported to be in sites near the surface with an A value of 83×10^{-4} cm^{-1}, [22] similar to what we observe. In some cases for InP:Mn nanoparticles, a second, weaker sextet is present as a set of shoulders on the main peaks with a hyperfine splitting constant closer to 90×10^{-4} cm^{-1}, which may indeed be due to surface bound Mn ions. Altogether, these data are consistent with varying Mn sites, some being surface bound and others located near the surface of the particles or in a distorted (or interstitial) environment. Indeed, the presence of a distorted environment would be consistent with the decrease in crystallinity found upon increasing Mn concentration in our InP:Mn nanoparticles. It should also be noted that the EPR signals contain a relatively larger isotropic component as compared to the hyperfine pattern for samples with high Mn content, especially in the Mn(III) doped samples, where more incorporation was found. This kind of observation is similar to that of previous reports, which attributed this larger isotropic component to Mn−Mn dipolar interactions present in the material.[47]

All InP:Mn samples exhibit a paramagnetic-like behavior in the temperature-dependent magnetic susceptibility data. After correcting for the background, an effective moment of 5.9 μ_B is determined from the data for the highest Mn(III)-doped sample, which is the expected value for the $S = 5/2$ spin state of Mn^{2+}. Also, the effective moments determined for the lower Mn(II) and Mn(III)-doped samples are consistent with the $S = 5/2$ spin state, although the large experimental uncertainties arising from the data preclude a more definitive conclusion. In contrast, in nanoparticles of InAs:Mn where Mn(II) was used as the dopant ion, a reduced moment, corresponding more nearly to 4 unpaired spins ($S = 2$) was found, despite the fact that the EPR data suggested a classic 5/2 spin system.[35] This reduced moment was attributed to n-type doping and/or donor−acceptor interactions between the impurity ions and antisite As.[35] These phenomena are also known to promote antiferromagnetic exchange between Mn ions. Indeed, negative θ values were

---

(44) Szczytko, J.; Twardowski, A.; Palczewska, M.; Jabłoński, R.; Furdyna, J.; Munekata, H. *Phys. Rev. B* **2001**, *63*, 085315/1−5.

(45) Macieja, B.; Korona, K. P.; Piersa, M.; Witowski, A. M.; Wasik, D.; Wysmołek, A.; Strezelecka, G.; Hruban, A.; Surma, B.; Palczewska, M.; Kamińska, M.; Twardowski, A. *Acta Phys. Pol., A* **2003**, *103*, 637−642.

(46) Kreissl, J.; Ulrici, W.; El-Metoui, M.; Vasson, A. M.; Vasson, A.; Gavaix, A. *Phys. Rev. B* **1996**, *54*, 10508−10515.

(47) Zając, M.; Doradziński, R.; Gosk, J.; Szczytko, J.; Lefeld-Sosnowska, M.; Kamińska, M.; Palczewska, M.; Grzanka.; Gębicki, W. *Appl. Phys. Lett.* **2001**, *78*, 1276−1278.

(48) Bleekrode, R.; Dieleman, J.; Vegter, H. J. *Phys. Lett.* **1962**, *2*, 355−356.

(49) Van Wierengen, J. S. *Discuss. Faraday Soc.* **1955**, *19*, 118−126.

(50) van Gisbergen, S. J. C. H. M.; Godlewski, M.; Gregorkiewicz, T.; Ammerlaan, C. A. J. *Phys. Rev. B* **1991**, *44*, 3012−3019.

found for all of the InAs:Mn nanomaterials studied, and the corresponding nearest-neighbor coupling constants, ranging from -2 to -4 K, are indicative of weak antiferromagnetic exchange. On the other hand, the nearest-neighbor coupling between Mn spins in the DMS25III-A nanoparticles is less than -0.4 K, an order of magnitude smaller. This value, when combined with the uncertainty in θ, suggests that the coupling between Mn spins is very weak or even nonexistent. This is not surprising as the Mn spins will be spatially isolated for such low concentrations of Mn and thus the probability of Mn being nearest and next-nearest neighbors in the zinc blende structure is extremely small. However, the EPR data suggest that in some samples, Mn−Mn interactions are present, as reflected in the isotropic component to the signal. The disparity between these sets of magnetic data may be a reflection of the multiple environments (inhomogeneity) in the samples, and the relative sensitivities of the instrumentation.

The absence of ferromagnetic exchange in the InP:Mn nanocrystals may be attributed to a number of different factors. If the Mn centers are in a highly distorted environment, the extent of hybridization with the rest of the lattice may be considerably limited, resulting in trapping of the hole in the valence band. Likewise, quantum confinement effects associated with these small particles would be expected to have a similar influence. Even though theoretical predictions indicated a lower limit of diameter of about 2.5 nm for retaining half-metallicity in GaAs:Mn,[16] this limit is a sensitive function of the hybridization within the material, which is expected to be quite different for InP relative to GaAs. It is also possible that the holes generated upon Mn(III) incorporation may have migrated to the surface and recombined with surface defects, thereby reducing the extent of *p*-doping and shutting down the mechanism of carrier induced ferromagnetic exchange. Although the upper value of holes achievable in these samples is equivalent to $\sim 10^{20}$ holes/cm^3 (based on the maximum number of 6 Mn ions per nanoparticle), which is adequate to induce ferromagnetic exchange in bulk materials, the limited number of holes in each nanoparticle may be insufficient, even if they are not trapped.[4] Finally, there may just be an insufficient number of Mn ions within each nanoparticle to promote ferromagnetic exchange and the observation of bulklike ferromagnetic behavior, as DMS25III-A had less than 6 Mn per particle and the other samples studied had less than 1 Mn per particle on the average.

Conclusions

Trivalent Mn precursors have been employed for the production of Mn^{2+} doped InP nanoparticles by an isovalent doping strategy. Despite the relatively high Mn concentration achieved with Mn(III) precursors and the large concentration of holes potentially generated, ferromagnetic exchange is not observed. However, this methodology may prove fruitful for generation of ferromagnetic DMS materials in the future if improved crystallinity can be achieved (i.e., Mn can be homogeneously incorporated into the lattice) and hole-recombination sites at the particle surface eliminated. Indeed, GaAs:Mn is a particularly good target, since the $d^5 + h$ neutral acceptor site that is associated with ferromagnetic exchange is well established in the bulk system.

Acknowledgment. This work is supported by an NSF-CAREER award (DMR-0094273) and the Institute for Manufacturing Research at Wayne State University. The microscopy in this publication was performed in the University of Michigan EMAL on the JEOL 2010F, which was purchased under NSF grant DMR-9871177. We thank John Mansfield and Corinna Wauchope (University of Michigan-EMAL) for their assistance with TEM studies.

Supporting Information Available: Temperature-dependent magnetic susceptibility data for all samples including pure InP nanoparticle samples plotted as a function of the inverse temperature and EPR data for InP:Mn nanoparticles before and after coating with another shell of InP (pdf). This material is available free of charge via the Internet at http://pubs.acs.org.

CM048796E